Available online at www.sciencedirect.com
SCIENCE DIRECT®
Journal of Sound and Vibration 289 (2006) 421–449
JOURNAL OF SOUND AND VIBRATION
www.elsevier.com/locate/jsvi

Buckling and free vibration analyses of stiffened plates using the FSDT mesh-free method

L.X. Peng[a], K.M. Liew[b,c], S. Kitipornchai[a,*]

[a]*Department of Building and Construction, City University of Hong Kong, Tat Chee Avenue, Kowloon, Hong Kong, China*
[b]*Nanyang Centre for Supercomputing and Visualisation, Nanyang Technological University, 639798 Singapore*
[c]*School of Mechanical and Aerospace Engineering, Nanyang Technological University, 639798 Singapore*

Received 4 March 2004; received in revised form 7 January 2005; accepted 8 February 2005
Available online 10 May 2005

Abstract

This paper presents a mesh-free Galerkin method for the free vibration and stability analyses of stiffened plates via the first-order shear deformable theory (FSDT). The model of a stiffened plate is formed by (1) regarding the plate and the stiffener separately, (2) imposing displacement compatible conditions between the plate and the stiffener so that displacement fields of the stiffener can be expressed in terms of the mid-surface displacement of the plate, and (3) superimposing the strain energy of plate and stiffener. Because there are no meshes used in this method, the stiffeners can be placed anywhere on the plate and need not be placed along the mesh lines. Several numerical examples are computed by this method to show its accuracy and convergence. The present results demonstrate good agreement with the existing solutions given by other researchers and the ANSYS. Influences of support size and order of the complete basis functions on the numerical accuracy are also investigated.

1. Introduction

A plate stiffened by ribs can achieve greater strength with relatively less material, which improves the strength/weight ratio and makes the structure cost efficient. Eccentrically stiffened plates have been widely used in all kinds of circumstances such as bridges, ship hulls or decks,

*Corresponding author.
E-mail address: bcskit@cityu.edu.hk (S. Kitipornchai).

0022-460X/$ - see front matter © 2005 Elsevier Ltd. All rights reserved.
doi:10.1016/j.jsv.2005.02.023

aircraft structures, etc. To make full use of the stiffness provided by stiffeners, they are often attached to plates along the main load-carrying directions.

Many researches have been carried out for the analysis of stiffened plates. The early researchers converted the stiffened plate to a single plate of constant thickness. The stiffeners are turned to an addition layer attached to the original plate. This is the so-called orthotropic model [1]. Another early model is the grillage models [2]. These models were simple in formulation but did not achieve satisfying results in solving generalized stiffened plate problems. To improve it, subsequent researchers tended to consider the stiffened plate as a composite structure, which combines the plate and stiffeners by imposing the displacement compatible conditions.

In stability analysis of stiffened plates, Bryan [3] first used energy criteria to study the stability of stiffened plates under uniform compression. Timoshenko and Gere [4] studied the rectangular plates stiffened by longitudinal and transverse ribs and gave the numerical tables of buckling loads. To keep the stiffened plate from local buckling, Klitchieff [5] found an expression to determine the minimum size of longitudinal stiffeners. Along with the development of computer techniques, numerical methods such as the finite strip method and the finite element method are introduced into the stability analysis. Turvey [6] first employed the finite strip method for stability analysis of stiffened plates. Yoshida and Maegawa [7], and Cheung and Delcourt [8] also used the finite strip method to study elastic stability and vibrations of stiffened plates. Buckling analysis of plates was also studied using the Ritz or Rayleigh–Ritz method [9–13]. In application of the finite element method to stability analysis stiffened plates, Mukhopadhyay and Mukherjee [14], Guo and Harik [15], Rikards et al. [16], and Barik and Mukhopadhyay [17] had made their own contributions.

A review paper on thick plate vibration that has summarized most of the stiffened plate vibration till 1994 [18] was published. In vibration analysis of stiffened plates, researchers have proposed many methods including the methods based on the early orthotropic model [19] and the grillage models [20], the Ritz or Rayleigh–Ritz method [21–24], the matrix method [25], the finite difference method [26–28], and the finite element method [15,29].

Due to the advances of computers in the past decades, the numerical methods, especially the finite element methods (FEM), are applied extensively in industry. The FEMs are convenient and can be used to solve large, complex structures with all kinds of boundary conditions. Nevertheless, in the analysis of stiffened plates, the FEMs have disadvantages. In early FEMs for stiffened plates, the discretization of the plate must make the mesh lines coincide with the stiffeners, which limit the position of the stiffeners. Once the stiffener position is changed, the plate will need remeshing. Although later improvements in FEMs have wiped off this restriction and stiffeners need not be placed along the mesh lines, there is still one limit the FEM cannot overcome—the element. The inherent characteristic of the FEMs may become disadvantageous under some circumstances.

In recent years, some powerful computational methods, namely meshless or meshfree methods, have emerged [31–53]. Unlike the FEMs, which base their solutions on the elements, the meshless methods construct the approximation solution completely in terms of a set of orderly or scattered points that discretize the problem domain. This makes the meshless methods more applicable than the FEMs in many instances, such as moving boundary problem, cracks growth with arbitrary and complex paths, and phase transformation problem. In these cases, the FEMs inevitably have difficulties in dealing with the discontinuities at every stage of the evolution because these

discontinuities do not coincide with the original mesh lines. Obviously, remeshing will be needed in each step of the solution procedures, which can result in decline of accuracy and complexity in programming. Meshless methods base their approximation solution entirely on a set of nodes distributed in the problem domain. Without the meshes, the meshless methods avoid the above difficulties that FEM encountered.

The objectives of this paper are to propose an FSDT mesh-free method for buckling and free vibration analyses of rectangular stiffened plates and compare the present results with other numerical methods.

2. The mesh-free Galerkin method

Using a moving least-squares approximation, a function $u(\mathbf{x})$ defined in a domain Ω can be approximated by $u^b(\mathbf{x})$ in the sub-domain $\Omega_{\mathbf{x}}$. $u^b(\mathbf{x})$ is defined as

$$u^b(\mathbf{x}) = \sum_{j=1}^{m} p_j(\mathbf{x}) a_j(\mathbf{x}) = \mathbf{p}^{\mathrm{T}}(\mathbf{x})\mathbf{a}(\mathbf{x}), \tag{1}$$

where $p_j(\mathbf{x})$ are monomial basis functions, $a_j(\mathbf{x})$ are their coefficients, b is a dilation factor that measures the size of the support of nodes, and m is the number of the basis functions. The commonly used basis is linear basis:

$$\mathbf{p}^{\mathrm{T}} = [1, x] \text{ in 1D}, \ m = 2, \tag{2}$$

$$\mathbf{p}^{\mathrm{T}} = [1, x, y] \text{ in 2D}, \ m = 3 \tag{3}$$

or quadratic basis:

$$\mathbf{p}^{\mathrm{T}} = [1, x, x^2] \text{ in 1D}, \ m = 3, \tag{4}$$

$$\mathbf{p}^{\mathrm{T}} = [1, x, y, x^2, xy, y^2] \text{ in 2D}, \ m = 6. \tag{5}$$

The unknown coefficients $a_j(\mathbf{x})$ can be determined by minimizing a weighted discrete L_2 norm

$$J = \sum_{I=1}^{n} \varpi(\mathbf{x} - \mathbf{x}_I)[\mathbf{p}(\mathbf{x}_I)^{\mathrm{T}}\mathbf{a}(\mathbf{x}) - u_I]^2, \tag{6}$$

where $\varpi(\mathbf{x} - \mathbf{x}_I)$ or $\varpi_I(\mathbf{x})$ is the weight function associated with node I, n is the number of nodes in $\Omega_{\mathbf{x}}$, which make the weight function $\varpi_I(\mathbf{x}) > 0$, and u_I are the nodal parameters. Minimizing J in Eq. (6) with respect to $\mathbf{a}(\mathbf{x})$ leads to a set of linear

$$\mathbf{A}(\mathbf{x})\mathbf{a}(\mathbf{x}) = \mathbf{B}(\mathbf{x})\mathbf{u}, \tag{7}$$

where

$$\mathbf{A}(\mathbf{x}) = \sum_{I=1}^{n} \varpi(\mathbf{x} - \mathbf{x}_I)\mathbf{p}(\mathbf{x}_I)\mathbf{p}^{\mathrm{T}}(\mathbf{x}_I), \tag{8}$$

$$\mathbf{B}(\mathbf{x}) = [\varpi(\mathbf{x} - \mathbf{x}_1)\mathbf{p}(\mathbf{x}_1), \ldots, \varpi(\mathbf{x} - \mathbf{x}_n)\mathbf{p}(\mathbf{x}_n)]. \tag{9}$$

The coefficients $\mathbf{a}(\mathbf{x})$ are then obtained from Eq. (7):

$$\mathbf{a}(\mathbf{x}) = \mathbf{A}^{-1}(\mathbf{x})\mathbf{B}(\mathbf{x})\mathbf{u}. \tag{10}$$

Substituting Eq. (10) into Eq. (1), the approximation $u^b(\mathbf{x})$ can then be expressed in a standard form as

$$u^b(\mathbf{x}) = \sum_{I=1}^{n} N_I(\mathbf{x})u_I, \tag{11}$$

where the shape function $N_I(\mathbf{x})$ is given by

$$N_I(\mathbf{x}) = \mathbf{p}^{\mathrm{T}}(\mathbf{x})\mathbf{A}^{-1}(\mathbf{x})\mathbf{B}_I(\mathbf{x}). \tag{12}$$

From Eq. (9), we can obtain

$$\mathbf{B}_I(\mathbf{x}) = \varpi(\mathbf{x} - \mathbf{x}_I)\mathbf{p}(\mathbf{x}_I). \tag{13}$$

Thus, Eq. (12) can be rewritten as

$$N_I(\mathbf{x}) = \mathbf{p}^{\mathrm{T}}(\mathbf{x})\mathbf{A}^{-1}(\mathbf{x})\mathbf{p}(\mathbf{x}_I)\varpi(\mathbf{x} - \mathbf{x}_I). \tag{14}$$

3. Formulation for stiffened plate

The mesh-free model of a stiffened plate, shown in Fig. 1, is composed of a plate and two beams. The plate and the beams are discretized by a set of nodes. The degree of freedom (dof) of every node of plate is $(w_p, \varphi_{px}, \varphi_{py})$. The dofs of every node of x-stiffener and y-stiffener are (w_{sx}, φ_{sx}) and (w_{sy}, φ_{sy}), respectively. In our study, we neglect the in-plane bending of the stiffeners, and they have negligible torsional stiffness.

3.1. Displacements approximation

The displacements of the plate used in the mesh-free method can be approximated by

$$u_p(x, y, z) = -z\varphi_{px} = -z \sum_{I=1}^{n} N_I(x, y)\varphi_{pxI}, \tag{15}$$

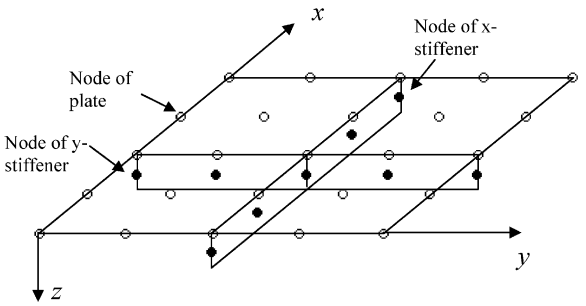

Fig. 1. Meshless model of a stiffened plate.

$$v_p(x,y,z) = -z\varphi_{py} = -z\sum_{I=1}^{n} N_I(x,y)\varphi_{pyI}, \tag{16}$$

$$w_p(x,y) = \sum_{I=1}^{n} N_I(x,y)w_{pI}, \tag{17}$$

where φ_{pxI}, φ_{pyx} and w_{pI} are the nodal parameters of plate. n is the number of nodes of the plate. The displacement field of the x-stiffener is

$$u_{sx}(x,z) = -z\varphi_{sx} = -z\sum_{I=1}^{N} \Phi_{xI}(x)\varphi_{sxI}, \tag{18}$$

$$w_{sx}(x) = \sum_{I=1}^{N} \Phi_{xI}(x)w_{sxI}, \tag{19}$$

where φ_{sxI} and w_{sxI} are the nodal parameters of the x-stiffener. N is the number of nodes of the stiffener. The displacement field of the y-stiffener is

$$v_{sy}(y,z) = -z\varphi_{sy} = -z\sum_{I=1}^{N} \Phi_{yI}(y)\varphi_{syI}, \tag{20}$$

$$w_{sy}(y) = \sum_{I=1}^{N} \Phi_{yI}(y)w_{syI}, \tag{21}$$

where φ_{syI} and w_{syI} are the nodal parameters of the y-stiffener. The shape functions $N_I(x,y)$, $\Phi_{xI}(x)$, and $\Phi_{yI}(y)$ are obtained from Eq. (14). A cubic spline function

$$\varpi(s) = \begin{cases} \frac{2}{3} - 4s^2 + 4s^3, & s \leqslant \frac{1}{2}, \\ \frac{4}{3} - 4s + 4s^2 - \frac{4}{3}s^3, & \frac{1}{2} < s \leqslant 1, \\ 0, & s > 1 \end{cases} \tag{22}$$

is used as the weight function. Quadratic basis $\mathbf{p}^{\mathrm{T}}$ is employed to compute the shape functions.

3.2. Transformation equations

As shown in Fig. 2, at every point along the connection line between the plate and the x-stiffener, we have

$$[\varphi_{px}] = [\varphi_{sx}], \tag{23}$$

$$[w_p] = [w_{sx}]. \tag{24}$$

From Eqs. (23) and (24), it can be deduced that

$$[\varphi_{px}]_i = [\varphi_{sx}]_i, \tag{25}$$

$$[w_p]_i = [w_{sx}]_i \quad (i = 1, \ldots, N) \tag{26}$$

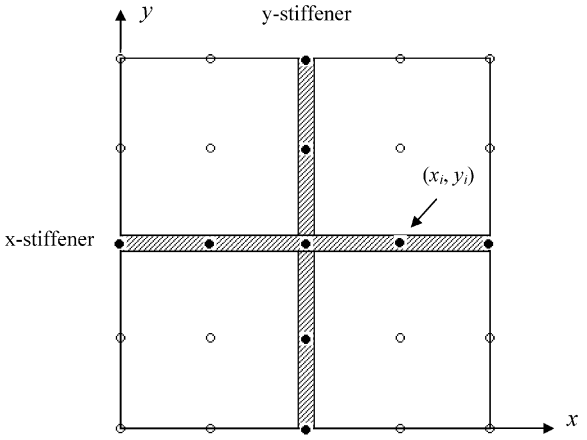

Fig. 2. Planform of the stiffened plate.

or

$$\varphi_{px}(x_i, y_i) = \varphi_{sx}(x_i, y_i), \tag{27}$$

$$w_p(x_i, y_i) = w_{sx}(x_i, y_i) \quad (i = 1, \ldots, N), \tag{28}$$

where N is the number of nodes of the x-stiffener. Remark: (x_i, y_i) can be any point on the plate that corresponds to the node (x_i, y_i) of the x-stiffeners. According to the mesh-free technique, Eqs. (27) and (28) are rewritten as

$$\sum_{I=1}^{n} N_I(x_i, y_i)\varphi_{pxI} = \sum_{J=1}^{N} \Phi_{xJ}(x_i)\varphi_{sxJ}, \tag{29}$$

$$\sum_{I=1}^{n} N_I(x_i, y_i)w_{pI} = \sum_{J=1}^{N} \Phi_{xJ}(x_i)w_{sxJ} \quad (i = 1, \ldots, N) \tag{30}$$

or in the matrix form

$$\mathbf{T}_{px\varphi}\boldsymbol{\delta}_{px\varphi} = \mathbf{T}_{sx\varphi}\boldsymbol{\delta}_{sx\varphi}, \tag{31}$$

where

$$\mathbf{T}_{px\varphi} = \begin{bmatrix} N_1(x_1, y_1) & N_2(x_1, y_1) & \cdots & N_n(x_1, y_1) \\ \vdots & \vdots & \ddots & \vdots \\ N_1(x_N, y_N) & N_2(x_N, y_N) & \cdots & N_n(x_N, y_N) \end{bmatrix}, \quad \boldsymbol{\delta}_{px\varphi} = \begin{bmatrix} \varphi_{px1} \\ \vdots \\ \varphi_{pxn} \end{bmatrix},$$

$$\mathbf{T}_{sx\varphi} = \begin{bmatrix} \Phi_{x1}(x_1) & \Phi_{x2}(x_1) & \cdots & \Phi_{xN}(x_1) \\ \vdots & \vdots & \ddots & \vdots \\ \Phi_{x1}(x_N) & \Phi_{x2}(x_N) & \cdots & \Phi_{xN}(x_N) \end{bmatrix}, \quad \boldsymbol{\delta}_{sx\varphi} = \begin{bmatrix} \varphi_{sx1} \\ \vdots \\ \varphi_{sxN} \end{bmatrix},$$

$$\mathbf{T}_{pw}\boldsymbol{\delta}_{pw} = \mathbf{T}_{sxw}\boldsymbol{\delta}_{sxw}, \tag{32}$$

where

$$\mathbf{T}_{pw} = \begin{bmatrix} N_1(x_1, y_1) & N_2(x_1, y_1) & \cdots & N_n(x_1, y_1) \\ \vdots & \vdots & \ddots & \vdots \\ N_1(x_N, y_N) & N_2(x_N, y_N) & \cdots & N_n(x_N, y_N) \end{bmatrix}, \quad \boldsymbol{\delta}_{pw} = \begin{bmatrix} w_{p1} \\ \vdots \\ w_{pn} \end{bmatrix},$$

$$\mathbf{T}_{sxw} = \begin{bmatrix} \Phi_{x1}(x_1) & \Phi_{x2}(x_1) & \cdots & \Phi_{xN}(x_1) \\ \vdots & \vdots & \ddots & \vdots \\ \Phi_{x1}(x_N) & \Phi_{x2}(x_N) & \cdots & \Phi_{xN}(x_N) \end{bmatrix}, \quad \boldsymbol{\delta}_{sxw} = \begin{bmatrix} w_{sx1} \\ \vdots \\ w_{sxN} \end{bmatrix}.$$

From Eqs. (31) and (32), we obtain

$$\boldsymbol{\delta}_{sx\varphi} = \mathbf{T}_{spx\varphi}\boldsymbol{\delta}_{px\varphi}, \tag{33}$$

where

$$\mathbf{T}_{spx\varphi} = \mathbf{T}_{sx\varphi}^{-1}\mathbf{T}_{px\varphi},$$

$$\boldsymbol{\delta}_{sxw} = \mathbf{T}_{spxw}\boldsymbol{\delta}_{pw} \tag{34}$$

where

$$\mathbf{T}_{spxw} = \mathbf{T}_{sxw}^{-1}\mathbf{T}_{pw}. \tag{35}$$

From the above Eqs. (33) and (34), we can form the transformation equation

$$\boldsymbol{\delta}_{sx} = \mathbf{T}_{spx}\boldsymbol{\delta}_{p}, \tag{36}$$

where

$$\boldsymbol{\delta}_{sx} = \begin{bmatrix} w_{sx1} \\ \varphi_{sx1} \\ 0 \\ w_{sx2} \\ \varphi_{sx2} \\ 0 \\ \vdots \\ w_{sxN} \\ \varphi_{sxN} \\ 0 \end{bmatrix}, \quad \boldsymbol{\delta}_{p} = \begin{bmatrix} w_{p1} \\ \varphi_{px1} \\ \varphi_{py1} \\ w_{p2} \\ \varphi_{px2} \\ \varphi_{py2} \\ \vdots \\ w_{pn} \\ \varphi_{pxn} \\ \varphi_{pyn} \end{bmatrix}$$

and $\mathbf{T}_{spx}$ is the $3N \times 3n$ matrix that transforms the nodal parameters of the x-stiffener to the nodal parameters of the plate.

Similarly, we can obtain the transformation equation

$$\boldsymbol{\delta}_{sy} = \mathbf{T}_{spy}\boldsymbol{\delta}_p \tag{37}$$

for the y-stiffener.

The transformation equations are the same for concentric stiffeners.

3.3. Stability analysis of stiffened plates

The stiffened plate in Fig. 1 is applied to the in-plane forces (Fig. 3). The potential energy of the plate can be expressed as

$$\begin{aligned}\Pi_p = {} & \frac{1}{2}\iint_{\Omega} \boldsymbol{\varepsilon}_p^{\mathrm{T}}\mathbf{D}\boldsymbol{\varepsilon}_p \,\mathrm{d}x\,\mathrm{d}y - \frac{1}{2}\iint_{\Omega} \boldsymbol{\beta}^{\mathrm{T}}\mathbf{R}\boldsymbol{\beta}\,\mathrm{d}x\,\mathrm{d}y \\ & + \iint_{\Omega} \frac{Gh_p}{2k}\left[\left(\frac{\partial w_p}{\partial x} - \varphi_{px}\right)^2 + \left(\frac{\partial w_p}{\partial y} - \varphi_{py}\right)^2\right]\mathrm{d}x\,\mathrm{d}y,\end{aligned} \tag{38}$$

where

$$\mathbf{D} = \frac{Eh_p^3}{12(1-\mu^3)}\begin{bmatrix} 1 & \mu & 0 \\ \mu & 1 & 0 \\ 0 & 0 & \dfrac{1-\mu}{2} \end{bmatrix}, \quad \boldsymbol{\beta} = \begin{bmatrix} \dfrac{\partial w_p}{\partial x} \\ \dfrac{\partial w_p}{\partial y} \end{bmatrix}, \tag{39}$$

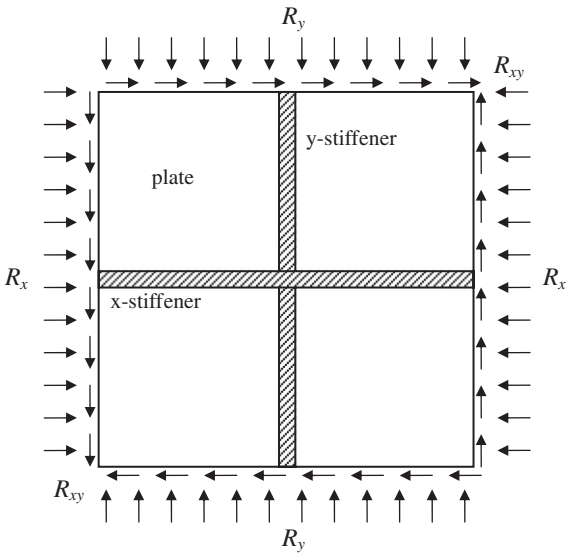

Fig. 3. Stiffened plate under in-plane compression.

and the in-plane load

$$\mathbf{R} = \begin{bmatrix} R_x & R_{xy} \\ R_{xy} & R_y \end{bmatrix}; \tag{40}$$

$k = 5/6$ is the shear correction factor and h_p is the thickness of the plate.

The potential energy of the x-stiffener is

$$\begin{aligned} \Pi_{sx} = & \int_l \frac{1}{2} E_{sx} I_{sx} \left(-\frac{\mathrm{d}\varphi_{sx}}{\mathrm{d}x} \right)^2 \mathrm{d}x - \frac{1}{2} \int_l \frac{R_x A_{sx}}{h_p} \left(\frac{\mathrm{d}w_{sx}}{\mathrm{d}x} \right)^2 \mathrm{d}x \\ & + \int_l \frac{1}{2} \frac{G_{sx} A_{sx}}{k} \left(\frac{\mathrm{d}w_{sx}}{\mathrm{d}x} - \varphi_{sx} \right)^2 \mathrm{d}x, \end{aligned} \tag{41}$$

where A_{sx} is the area of the cross section of the x-stiffener.

The potential energy of the y-stiffener is

$$\begin{aligned} \Pi_{sy} = & \int_l \frac{1}{2} E_{sy} I_{sy} \left(-\frac{\mathrm{d}\varphi_{sy}}{\mathrm{d}y} \right)^2 \mathrm{d}y - \frac{1}{2} \int_l \frac{R_y A_{sy}}{h_p} \left(\frac{\mathrm{d}w_{sy}}{\mathrm{d}y} \right)^2 \mathrm{d}y \\ & + \int_l \frac{1}{2} \frac{G_{sy} A_{sy}}{k} \left(\frac{\mathrm{d}w_{sy}}{\mathrm{d}y} - \varphi_{sy} \right)^2 \mathrm{d}y, \end{aligned} \tag{42}$$

where A_{sy} is the area of the cross section of the stiffener.

Therefore, the potential energy of the stiffened plate is

$$\Pi = \Pi_p + \Pi_{sx} + \Pi_{sy}. \tag{43}$$

Substituting Eqs. (15)–(21) into Eq. (43), we obtain

$$\begin{aligned} \Pi = & \tfrac{1}{2} \boldsymbol{\delta}_p^{\mathrm{T}} \mathbf{K}_p \boldsymbol{\delta}_p - \tfrac{1}{2} \boldsymbol{\delta}_p^{\mathrm{T}} \mathbf{G}_p \boldsymbol{\delta}_p + \tfrac{1}{2} \boldsymbol{\delta}_{sx}^{\mathrm{T}} \mathbf{K}_{sx} \boldsymbol{\delta}_{sx} - \tfrac{1}{2} \boldsymbol{\delta}_{sx}^{\mathrm{T}} \mathbf{G}_{sx} \boldsymbol{\delta}_{sx} \\ & + \tfrac{1}{2} \boldsymbol{\delta}_{sy}^{\mathrm{T}} \mathbf{K}_{sy} \boldsymbol{\delta}_{sy} - \tfrac{1}{2} \boldsymbol{\delta}_{sy}^{\mathrm{T}} \mathbf{G}_{sy} \boldsymbol{\delta}_{sy}, \end{aligned} \tag{44}$$

where

$$[\mathbf{K}_p]_{ij} = \iint_{\Omega} (\mathbf{B}_{bi}^{\mathrm{T}} \mathbf{D} \mathbf{B}_{bj} + \alpha \mathbf{B}_{si}^{\mathrm{T}} \mathbf{B}_{sj}) \, \mathrm{d}x \, \mathrm{d}y,$$

$$[\mathbf{K}_{sx}]_{ij} = \int_l (\mathbf{B}_{sxi}^{\mathrm{T}} E_{sx} I_{sx} \mathbf{B}_{sxj} + \alpha_{sx} \mathbf{B}_{sxsi}^{\mathrm{T}} \mathbf{B}_{sxsj}) \, \mathrm{d}x,$$

$$[\mathbf{K}_{sy}]_{ij} = \int_l (\mathbf{B}_{syi}^{\mathrm{T}} E_{sy} I_{sy} \mathbf{B}_{syj} + \alpha_{sy} \mathbf{B}_{sysi}^{\mathrm{T}} \mathbf{B}_{sysj}) \, \mathrm{d}y$$

and

$$\mathbf{B}_{bi} = \begin{bmatrix} 0 & -N_{i,x} & 0 \\ 0 & 0 & -N_{i,y} \\ 0 & -N_{i,y} & -N_{i,x} \end{bmatrix}, \quad \mathbf{B}_{si} = \begin{bmatrix} N_{i,x} & -N_i & 0 \\ N_{i,y} & 0 & -N_i \end{bmatrix},$$

$$\mathbf{B}_{sxi} = \begin{bmatrix} 0 & -\Phi_{xi,x} & 0 \end{bmatrix}, \quad \mathbf{B}_{sxsi} = \begin{bmatrix} \Phi_{xi,x} & -\Phi_{xi} & 0 \end{bmatrix},$$

$$\mathbf{B}_{syi} = \begin{bmatrix} 0 & 0 & -\Phi_{yi,y} \end{bmatrix}, \quad \mathbf{B}_{sysi} = \begin{bmatrix} \Phi_{yi,y} & 0 & -\Phi_{yi} \end{bmatrix},$$

$$\alpha = Gh_p/k, \quad \alpha_{sx} = G_{sx}A_{sx}/k, \quad \alpha_{sy} = G_{sy}A_{sy}/k,$$

$$[\mathbf{G}_p]_{ij} = \iint_{\Omega} \begin{bmatrix} R & 0 & 0 \\ 0 & 0 & 0 \\ 0 & 0 & 0 \end{bmatrix} \mathrm{d}x\,\mathrm{d}y, \tag{45}$$

$$R = R_x N_{i,x} N_{j,x} + R_y N_{i,y} N_{j,y} + R_{xy}(N_{i,x} N_{j,y} + N_{i,y} N_{j,x}),$$

$$[\mathbf{G}_{sx}]_{ij} = \frac{R_x A_{sx}}{h_p} \int_l \begin{bmatrix} \Phi_{xi,x}\Phi_{xj,x} & 0 \\ 0 & 0 \end{bmatrix} \mathrm{d}x, \tag{46}$$

$$[\mathbf{G}_{sy}]_{ij} = \frac{R_y A_{sy}}{h_p} \int_l \begin{bmatrix} \Phi_{yi,y}\Phi_{yj,y} & 0 \\ 0 & 0 \end{bmatrix} \mathrm{d}y. \tag{47}$$

Substituting Eqs. (36) and (37) into Eq. (44), we have

$$\begin{aligned} \Pi = {} & \tfrac{1}{2}\boldsymbol{\delta}_p^{\mathrm{T}}\mathbf{K}_p\boldsymbol{\delta}_p + \tfrac{1}{2}\boldsymbol{\delta}_p^{\mathrm{T}}\mathbf{T}_{spx}^{\mathrm{T}}\mathbf{K}_{sx}\mathbf{T}_{spx}\boldsymbol{\delta}_p + \tfrac{1}{2}\boldsymbol{\delta}_p^{\mathrm{T}}\mathbf{T}_{spy}^{\mathrm{T}}\mathbf{K}_{sy}\mathbf{T}_{spy}\boldsymbol{\delta}_p \\ & - \tfrac{1}{2}\boldsymbol{\delta}_p^{\mathrm{T}}\mathbf{G}_p\boldsymbol{\delta}_p - \tfrac{1}{2}\boldsymbol{\delta}_p^{\mathrm{T}}\mathbf{T}_{spx}^{\mathrm{T}}\mathbf{G}_{sx}\mathbf{T}_{spx}\boldsymbol{\delta}_p - \tfrac{1}{2}\boldsymbol{\delta}_p^{\mathrm{T}}\mathbf{T}_{spy}^{\mathrm{T}}\mathbf{G}_{sy}\mathbf{T}_{spy}\boldsymbol{\delta}_p \end{aligned} \tag{48}$$

or

$$\Pi = \tfrac{1}{2}\boldsymbol{\delta}_p^{\mathrm{T}}\mathbf{K}\boldsymbol{\delta}_p - \tfrac{1}{2}\boldsymbol{\delta}_p^{\mathrm{T}}\mathbf{G}\boldsymbol{\delta}_p, \tag{49}$$

where

$$\mathbf{K} = \mathbf{K}_p + \mathbf{T}_{spx}^{\mathrm{T}}\mathbf{K}_{sx}\mathbf{T}_{spx} + \mathbf{T}_{spy}^{\mathrm{T}}\mathbf{K}_{sy}\mathbf{T}_{spy},$$

$$\mathbf{G} = \mathbf{G}_p + \mathbf{T}_{spx}^{\mathrm{T}}\mathbf{G}_{sx}\mathbf{T}_{spx} + \mathbf{T}_{spy}^{\mathrm{T}}\mathbf{G}_{sy}\mathbf{T}_{spy}.$$

Invoking $\delta\Pi = 0$ results in the following equation:

$$(\mathbf{K} - \mathbf{G})\boldsymbol{\delta}_p = \mathbf{0}. \tag{50}$$

Assume

$$R_x = \alpha_1 R_y \quad \text{and} \quad R_x = \alpha_2 R_{xy}.$$

α_1 and α_2 are constants. Extracting R_x from $\mathbf{G}$, we obtain

$$(\mathbf{K} - R_x\mathbf{G}')\boldsymbol{\delta}_p = \mathbf{0}. \tag{51}$$

Solving this eigenvalue problem, the buckling load R_{cr} will be obtained. The critical value of the compressive stress is therefore given by

$$\sigma_{\mathrm{cr}} = \frac{R_{\mathrm{cr}}}{h_p}, \tag{52}$$

where h_p is the thickness of the plate.

3.4. Free vibration analysis of stiffened plates

The displacement field of the plate is

$$u_p(x,y,z,t) = -z\varphi_{px}(t) = -z\sum_{I=1}^{n} N_I(x,y)\varphi_{pxI}(t), \tag{53}$$

$$v_p(x,y,z,t) = -z\varphi_{py}(t) = -z\sum_{I=1}^{n} N_I(x,y)\varphi_{pyI}(t), \tag{54}$$

$$w_p(x,y,t) = \sum_{I=1}^{n} N_I(x,y)w_{pI}(t). \tag{55}$$

The displacement field of the x-stiffener is

$$u_{sx}(x,z,t) = -z\varphi_{sx} = -z\sum_{I=1}^{N} \Phi_{xI}(x)\varphi_{sxI}(t), \tag{56}$$

$$w_{sx}(x,t) = \sum_{I=1}^{N} \Phi_{xI}(x)w_{sxI}(t). \tag{57}$$

The displacement field of the y-stiffener is

$$v_{sy}(y,z,t) = -z\varphi_{sy}(t) = -z\sum_{I=1}^{N} \Phi_{yI}(y)\varphi_{syI}(t), \tag{58}$$

$$w_{sy}(y,t) = \sum_{I=1}^{N} \Phi_{yI}(y)w_{syI}(t). \tag{59}$$

The potential energy of the plate can be expressed as

$$\begin{aligned}\Pi_p = {} & \frac{1}{2}\iint_{\Omega} \boldsymbol{\varepsilon}_p^{\mathrm{T}}\mathbf{D}\boldsymbol{\varepsilon}_p \,\mathrm{d}x\,\mathrm{d}y + \frac{1}{2}\iint_{\Omega}\int_{-h_p/2}^{h_p/2} \mathbf{U}_p\rho\ddot{\mathbf{U}}_p \,\mathrm{d}z\,\mathrm{d}x\,\mathrm{d}y \\ & + \iint_{\Omega} \frac{Gh_p}{2k}\left[\left(\frac{\partial w_p}{\partial x} - \varphi_{px}\right)^2 + \left(\frac{\partial w_p}{\partial y} - \varphi_{py}\right)^2\right]\mathrm{d}x\,\mathrm{d}y,\end{aligned} \tag{60}$$

where

$$\boldsymbol{\varepsilon}_p = \begin{bmatrix} -\dfrac{\partial\varphi_{px}}{\partial x} \\ -\dfrac{\partial\varphi_{py}}{\partial y} \\ -\left(\dfrac{\partial\varphi_{px}}{\partial y} + \dfrac{\partial\varphi_{py}}{\partial x}\right) \end{bmatrix} = \sum_{I=1}^{n} \begin{bmatrix} 0 & -N_{I,x} & 0 \\ 0 & 0 & -N_{I,y} \\ 0 & -N_{I,y} & -N_{I,x} \end{bmatrix} \begin{bmatrix} w_{pI}(t) \\ \varphi_{pxI}(t) \\ \varphi_{pyI}(t) \end{bmatrix}, \tag{61}$$

$$\mathbf{D} = \frac{Eh_p^3}{12(1-\mu^3)} \begin{bmatrix} 1 & \mu & 0 \\ \mu & 1 & 0 \\ 0 & 0 & \dfrac{1-\mu}{2} \end{bmatrix},$$

$$\mathbf{U}_p = \begin{bmatrix} w_p \\ u_p \\ v_p \end{bmatrix} = \sum_{I=1}^{n} \begin{bmatrix} N_I(x,y) & 0 & 0 \\ 0 & -zN_I(x,y) & 0 \\ 0 & 0 & -zN_I(x,y) \end{bmatrix} \begin{bmatrix} w_{pI}(t) \\ \varphi_{pxI}(t) \\ \varphi_{pyI}(t) \end{bmatrix}, \tag{62}$$

$$\ddot{\mathbf{U}}_p = \begin{bmatrix} \ddot{w}_p \\ \ddot{u}_p \\ \ddot{v}_p \end{bmatrix} = \sum_{I=1}^{n} \begin{bmatrix} N_I(x,y) & 0 & 0 \\ 0 & -zN_I(x,y) & 0 \\ 0 & 0 & -zN_I(x,y) \end{bmatrix} \begin{bmatrix} \ddot{w}_{pI}(t) \\ \ddot{\varphi}_{pxI}(t) \\ \ddot{\varphi}_{pyI}(t) \end{bmatrix} \tag{63}$$

and ρ is the density of the plate.

The potential energy of the x-stiffener is

$$\begin{aligned} \Pi_{sx} = & \int_l \frac{1}{2} E_{sx} I_{sx} \left(-\frac{\mathrm{d}\varphi_{sx}}{\mathrm{d}x} \right)^2 \mathrm{d}x + \frac{1}{2} \int_l \int_{-h_{sx}/2}^{h_{sx}/2} \mathbf{U}_{sx} \rho_{sx} \ddot{\mathbf{U}}_{sx} W_{sx} \, \mathrm{d}z \, \mathrm{d}x \\ & + \int_l \frac{1}{2} \frac{G_{sx} A_{sx}}{k} \left(\frac{\mathrm{d}w_{sx}}{\mathrm{d}x} - \varphi_{sx} \right)^2 \mathrm{d}x, \end{aligned} \tag{64}$$

where

$$\mathbf{U}_{sx} = \begin{bmatrix} w_{sx} \\ u_{sx} \end{bmatrix} = \sum_{J=1}^{N} \begin{bmatrix} \Phi_{xJ}(x) & 0 \\ 0 & -z\Phi_{xJ}(x) \end{bmatrix} \begin{bmatrix} w_{sxJ}(t) \\ \varphi_{sxJ}(t) \end{bmatrix}, \tag{65}$$

$$\ddot{\mathbf{U}}_{sx} = \begin{bmatrix} \ddot{w}_{sx} \\ \ddot{u}_{sx} \end{bmatrix} = \sum_{J=1}^{N} \begin{bmatrix} \Phi_{xJ}(x) & 0 \\ 0 & -z\Phi_{xJ}(x) \end{bmatrix} \begin{bmatrix} \ddot{w}_{sxJ}(t) \\ \ddot{\varphi}_{sxJ}(t) \end{bmatrix} \tag{66}$$

and ρ_{sx} is the density; W_{sx} is the width of the cross section; h_{sx} is the depth.

The potential energy of the y-stiffener is

$$\begin{aligned} \Pi_{sy} = & \int_l \frac{1}{2} E_{sy} I_{sy} \left(-\frac{\mathrm{d}\varphi_{sy}}{\mathrm{d}y} \right)^2 \mathrm{d}y + \frac{1}{2} \int_l \int_{-h_{sy}/2}^{h_{sy}/2} \mathbf{U}_{sy} \rho_{sy} \ddot{\mathbf{U}}_{sy} W_{sy} \, \mathrm{d}z \, \mathrm{d}y \\ & + \int_l \frac{1}{2} \frac{G_{sy} A_{sy}}{k} \left(\frac{\mathrm{d}w_{sy}}{\mathrm{d}y} - \varphi_{sy} \right)^2 \mathrm{d}y, \end{aligned} \tag{67}$$

where

$$\mathbf{U}_{sy} = \begin{bmatrix} w_{sy} \\ u_{sy} \end{bmatrix} = \sum_{J=1}^{N} \begin{bmatrix} \Phi_{yJ}(y) & 0 \\ 0 & -z\Phi_{yJ}(y) \end{bmatrix} \begin{bmatrix} w_{syJ}(t) \\ \varphi_{syJ}(t) \end{bmatrix}, \tag{68}$$

$$\ddot{\mathbf{U}}_{sy} = \begin{bmatrix} \ddot{w}_{sy} \\ \ddot{u}_{sy} \end{bmatrix} = \sum_{J=1}^{N} \begin{bmatrix} \Phi_{yJ}(y) & 0 \\ 0 & -z\Phi_{yJ}(y) \end{bmatrix} \begin{bmatrix} \ddot{w}_{syJ}(t) \\ \ddot{\varphi}_{syJ}(t) \end{bmatrix} \tag{69}$$

and ρ_{sy} is the density; W_{sy} is the width of the cross section; h_{sx} is the depth.

Therefore, the potential energy of the stiffened plate is

$$\Pi = \Pi_p + \Pi_{sx} + \Pi_{sy}. \tag{70}$$

Substituting Eqs. (53)–(59), (63), (66), and (69) into Eq. (70), we obtain

$$\begin{aligned} \Pi = {} & \tfrac{1}{2}\boldsymbol{\delta}_p^{\mathrm{T}}\mathbf{K}_p\boldsymbol{\delta}_p + \tfrac{1}{2}\boldsymbol{\delta}_p^{\mathrm{T}}\mathbf{M}_p\ddot{\boldsymbol{\delta}}_p + \tfrac{1}{2}\boldsymbol{\delta}_{sx}^{\mathrm{T}}\mathbf{K}_{sx}\boldsymbol{\delta}_{sx} + \tfrac{1}{2}\boldsymbol{\delta}_{sx}^{\mathrm{T}}\mathbf{M}_{sx}\ddot{\boldsymbol{\delta}}_{sx} \\ & + \tfrac{1}{2}\boldsymbol{\delta}_{sy}^{\mathrm{T}}\mathbf{K}_{sy}\boldsymbol{\delta}_{sy} + \tfrac{1}{2}\boldsymbol{\delta}_{sy}^{\mathrm{T}}\mathbf{M}_{sy}\ddot{\boldsymbol{\delta}}_{sy}, \end{aligned} \tag{71}$$

where

$$[\mathbf{M}_p]_{ij} = \iint_{\Omega} \begin{bmatrix} \rho h_p N_i N_j & 0 & 0 \\ 0 & \dfrac{\rho h_p^3}{12} N_i N_j & 0 \\ 0 & 0 & \dfrac{\rho h_p^3}{12} N_i N_j \end{bmatrix} \mathrm{d}x\,\mathrm{d}y, \tag{72}$$

$$[\mathbf{M}_{sx}]_{ij} = \int_l \rho_{sx} \begin{bmatrix} A_{sx}\Phi_{xi}\Phi_{xj} & 0 \\ 0 & I_{sx}\Phi_{xi}\Phi_{xj} \end{bmatrix} \mathrm{d}x, \tag{73}$$

$$[\mathbf{M}_{sy}]_{ij} = \int_l \rho_{sy} \begin{bmatrix} A_{sy}\Phi_{yi}\Phi_{yj} & 0 \\ 0 & I_{sy}\Phi_{yi}\Phi_{yj} \end{bmatrix} \mathrm{d}y, \tag{74}$$

and $\mathbf{K}_p$, $\mathbf{K}_{sx}$, and $\mathbf{K}_{sy}$ are the same as those in Eq. (44).

From Eq. (36), we obtain

$$\ddot{\boldsymbol{\delta}}_{sx} = \mathbf{T}_{spx}\ddot{\boldsymbol{\delta}}_p. \tag{75}$$

Similarly, we have

$$\ddot{\boldsymbol{\delta}}_{sy} = \mathbf{T}_{spy}\ddot{\boldsymbol{\delta}}_p. \tag{76}$$

Substituting Eqs. (75) and (76) into Eq. (71), we have

$$\Pi = \tfrac{1}{2}\boldsymbol{\delta}_p^{\mathrm{T}}\mathbf{K}\boldsymbol{\delta}_p + \tfrac{1}{2}\boldsymbol{\delta}_p^{\mathrm{T}}\mathbf{M}\ddot{\boldsymbol{\delta}}_p, \tag{77}$$

where

$$\mathbf{K} = \mathbf{K}_p + \mathbf{T}_{spx}^{\mathrm{T}}\mathbf{K}_{sx}\mathbf{T}_{spx} + \mathbf{T}_{spy}^{\mathrm{T}}\mathbf{K}_{sy}\mathbf{T}_{spy} \tag{78}$$

and

$$\mathbf{M} = \mathbf{M}_p + \mathbf{T}_{spx}^{\mathrm{T}}\mathbf{M}_{sx}\mathbf{T}_{spx} + \mathbf{T}_{spy}^{\mathrm{T}}\mathbf{M}_{sy}\mathbf{T}_{spy}. \tag{79}$$

Invoking $\delta\Pi = 0$ results in the following linear equation:

$$\mathbf{K}\boldsymbol{\delta}_p + \mathbf{M}\ddot{\boldsymbol{\delta}}_p = \mathbf{0}. \tag{80}$$

Solving the corresponding eigenvalue problem

$$(\mathbf{K} - \omega^2\mathbf{M})\boldsymbol{\delta}_0 = \mathbf{0}, \tag{81}$$

we will obtain the frequencies of the stiffened plate free vibration.

3.5. Enforcement of essential boundary conditions

Due to lack of the Kronecker delta properties in meshless shape functions, imposition of the essential boundary conditions is usually a difficulty in the meshless method. Here, we use the full transformation method introduced by Ren and Liew [39] to enforce the essential boundary conditions.

4. Results and discussion

4.1. Validation studies

Free vibration of a simply supported rectangular stiffened plate with one central stiffener (Fig. 4) is considered. Young's modulus and Poisson's ratio of the plate and stiffener are 211 GPa and 0.3, respectively. The density is $7830\,\mathrm{kg/m^3}$. Frequencies obtained by the authors are compared with those given by other researchers in Table 1. The agreement is good.

The fundamental frequency obtained under different scaling factor $d_{\max}$ and different completeness order of basis function N_c is shown in Fig. 5, compared with the result given by Aksu [27]. The meshless scheme is chosen to be 13×13 nodes for the plate and 13 nodes for stiffener.

For circular support, the scaling factor $d_{\max}$ is defined as

$$d_{\max} = \frac{r}{h_m}, \tag{82}$$

where r is the radius of the support of the node and h_m is the distance between two neighbouring nodes. Here, we use rectangular support; so the scaling factors $d^x_{\max}$ and $d^y_{\max}$ are defined as

$$d^x_{\max} = \frac{l_x}{h_{mx}} \quad \text{and} \quad d^y_{\max} = \frac{l_y}{h_{my}}, \tag{83}$$

where l_x and l_y are the lengths of the rectangular support in x and y directions, respectively; h_{mx} and h_{my} are the distances between two neighbouring nodes in x and y directions, respectively. For convenience, we choose $d^x_{\max} = d^y_{\max}$.

From Fig. 5, one can find that larger support size (denoted by $d_{\max}$ for certain number of nodes) gives relatively more accurate results if the completeness orders are the same. Higher completeness order (denoted by N_c) basis function needs larger support to obtain better results.

The study of convergence is introduced by increasing the nodes that discretize the stiffened plate and the scaling factor $d_{\max}$ under different completeness order of basis function N_c.

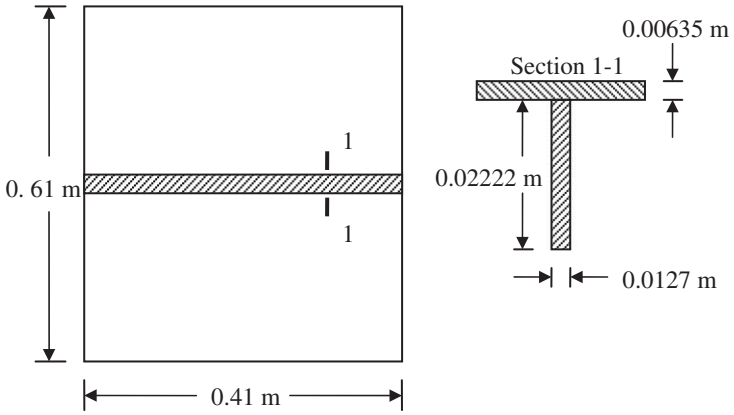

Fig. 4. Simply supported stiffened plate with single central stiffener.

Table 1
Frequencies (Hz) of the simply supported stiffened plate with single stiffener (Fig. 4)

Mode	Ref. [27]	Ref. [29]	Ref. [30]	Ref. [55]	Present results
1	254.94	257.05	253.59	250.27	254.45
2	269.46	272.10	282.02	274.49	265.86
3	511.64	524.70	513.50	517.77	520.14

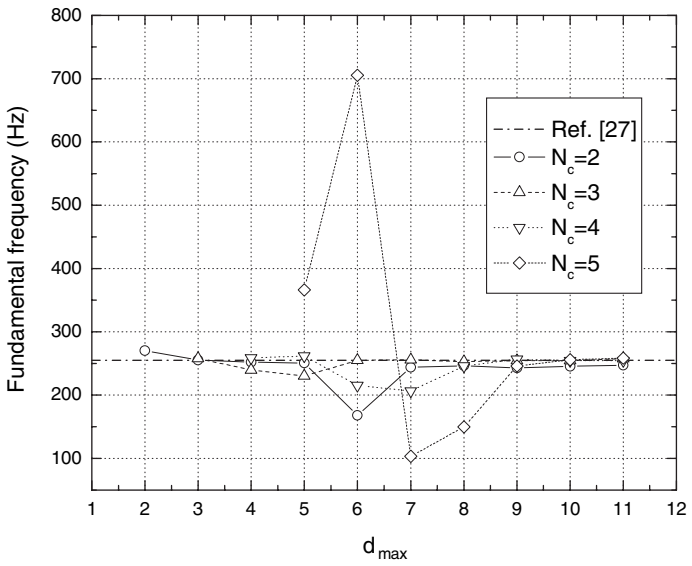

Fig. 5. Fundamental frequency variation of eccentrically stiffened plate under different $d_{\max}$ and N_c.

Figs. 6–9 show the variation of the fundamental frequency of the eccentrically stiffened plate with different nodes and $d_{\max}$ under different N_c. The solution given by Aksu [27] is also shown in the figures for comparison. We noted from the existing literature that $d_{\max}$ ranges from 2 to 4 and $N_c = 2$ can furnish satisfactory results for most plate problems.

It is noted in Figs. 6–9 that for a certain $d_{\max}$, the solution converges when the number of nodes increases. Higher completeness order needs larger support size to make the solution converge.

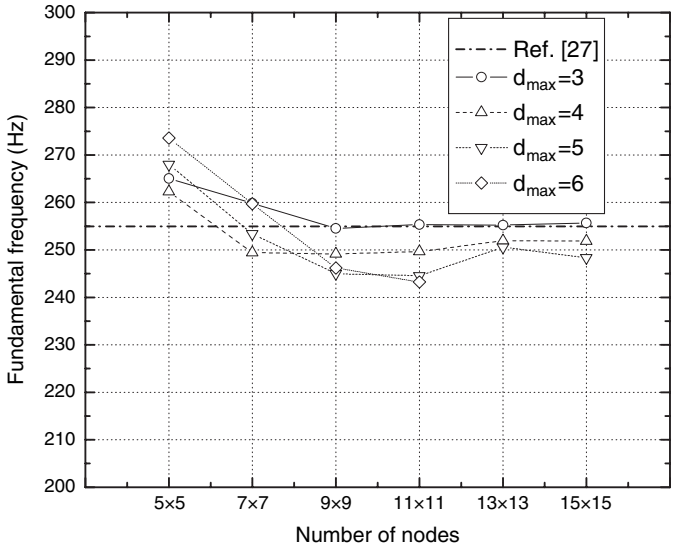

Fig. 6. Variation of the fundamental frequency of the eccentrically stiffened plate, $N_c = 2$.

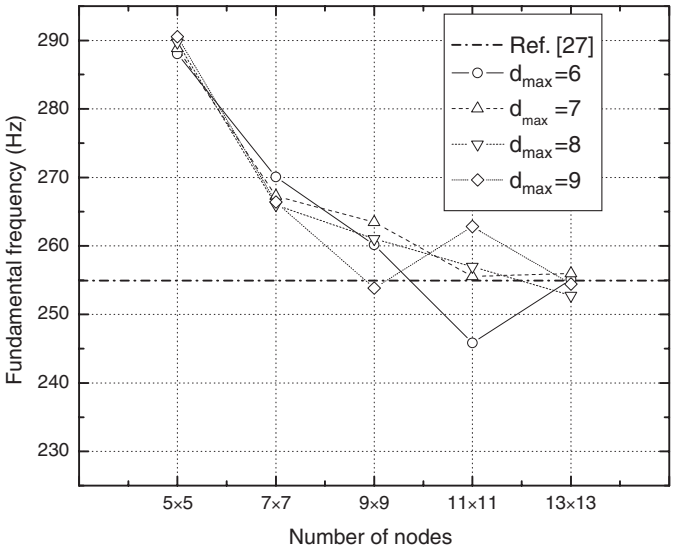

Fig. 7. Variation of the fundamental frequency of the eccentrically stiffened plate, $N_c = 3$.

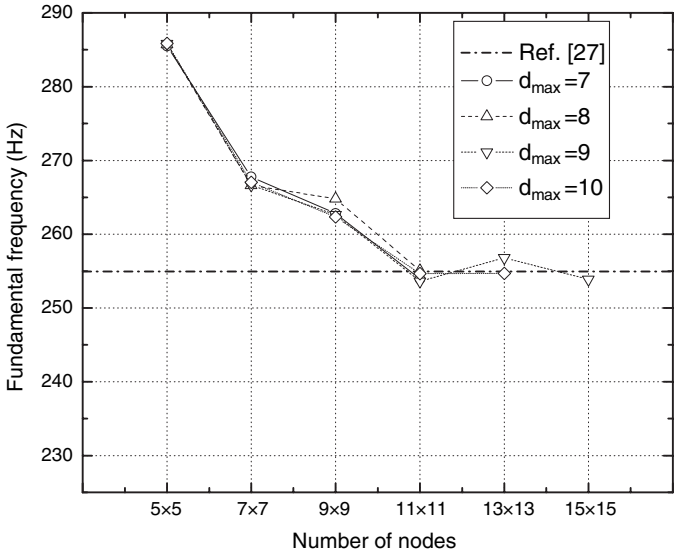

Fig. 8. Variation of the fundamental frequency of the eccentrically stiffened plate, $N_c = 4$.

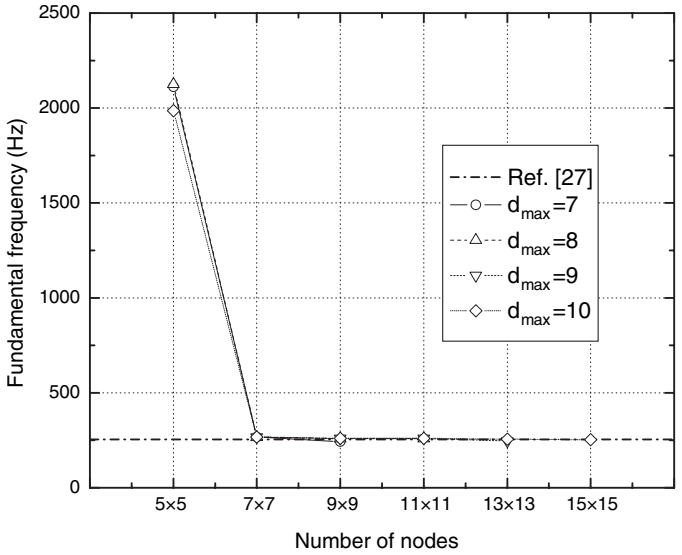

Fig. 9. Variation of the fundamental frequency of the eccentrically stiffened plate, $N_c = 5$.

Moreover, higher completeness order of basis function can achieve better convergence characteristic than the lower order of basis functions.

By analyzing the convergence figures, we found that the basis function of $N_c = 2$ can help us obtain results good enough compared to the solution given by Ref. [27] at the lowest cost of computation. This result well coincides with the existing solutions. Therefore, all the following examples are computed using the basis function of $N_c = 2$ and $d_{\max} = 3.5$ for the stiffened plate

problems considered, and $N_c = 2$ and $d_{\max}$ ranges from 2 to 4 are also the recommended values for stiffened plate problems.

4.2. Free vibration of a fully clamped square stiffened plate

Free vibration of a fully clamped square plate stiffened by a single stiffener (Fig. 10) is examined. Young's modulus and Poisson's ratio of the plate and stiffener are 68.7 GPa and 0.3, respectively. The density is 2820 kg/m^3. The frequencies of 10 modes are listed in Table 2, compared with the experimental results given by Olson et al. [54] and the ANSYS results. In order to use ANSYS in our modelling, we considered the stiffened plate as a composite structure that combines the plate and stiffeners by imposing the displacement compatible conditions. We have used Shell 63 element to model the plate and Beam 4 element to model the stiffeners.

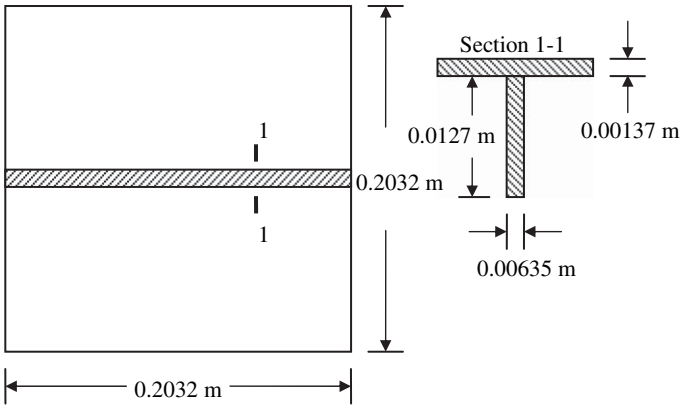

Fig. 10. Clamped stiffened square plate with single central stiffener.

Table 2
Experimental and numerical frequencies (Hz) of the clamped stiffened plate with single stiffener (Fig. 10)

Mode	Experimental results (Ref. [54])	Present results	Relative errors to experimental results (%)	ANSYS
1	689	574.11	16.675	573.537
2	725	754.35	−4.048	755.03
3	961	846.55	11.909	838.306
4	986	993.47	−0.758	980.143
5	1376	1293.8	5.974	1272.27
6	1413	1402.8	0.722	1372.97
7	1512	1650.3	−9.147	1641.67
8	1770	1805.1	−1.983	1861.87
9	1995	1897.2	4.902	1869.84
10	2069	1904.4	7.956	1873.52

4.3. Free vibration of a simply supported rectangular stiffened plate with two stiffeners

Free vibration of a simply supported rectangular plate stiffened eccentrically by two stiffeners (Fig. 11) is considered. Both plate and stiffener are made of the same material with the elastic modulus $= 3 \times 10^7$ Pa and Poisson's ratio $= 0.3$. The density is 2820 kg/m^3. The authors' solution is compared with the results from ANSYS in Table 3. The same ANSYS model used in Section 4.2 is employed in this case.

The frequencies obtained by the authors when the thickness of the plate increases to 1.5 m, which means the thickness-to-length ratio of the plate is increased to 0.05, are listed in Table 4 compared to the ANSYS results. The frequencies obtained by the authors when the thickness of the plate increases to 3.0 m, are listed in Table 5 compared to the ANSYS results.

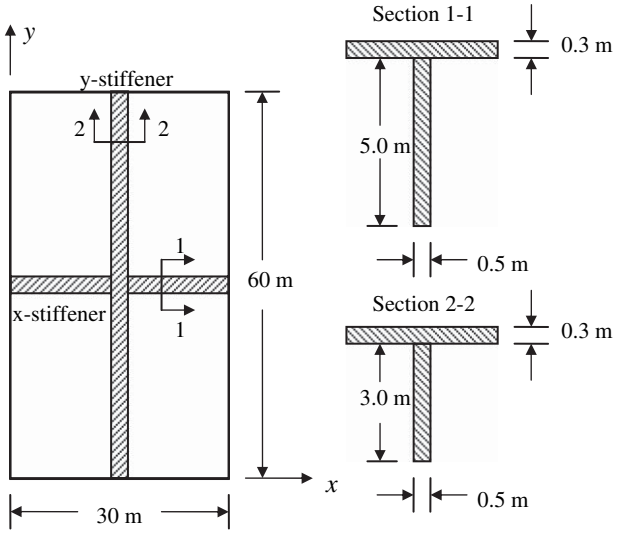

Fig. 11. The stiffened rectangular plate with two stiffeners.

Table 3
Frequencies (Hz) of the simply supported stiffened plate with two stiffeners (Fig. 11)

Mode	ANSYS results	Present results	Relative errors to ANSYS results (%)
1	0.0812595	0.081653	−0.48
2	0.0849575	0.085652	−0.82
3	0.103598	0.10003	3.44
4	0.109025	0.1028	5.71
5	0.129271	0.13118	−1.48
6	0.14064	0.14371	−2.18
7	0.153224	0.15411	−0.58
8	0.160818	0.16036	0.28
9	0.20927	0.19835	5.22
10	0.219804	0.20333	7.49

Table 4
Frequencies (Hz) of the simply supported stiffened plate with two stiffeners (Fig. 11, the thickness of the plate increases to 1.5 m)

Mode	ANSYS results	Present results	Relative errors to ANSYS results (%)
1	0.162099	0.15888	1.99
2	0.189169	0.19288	−1.96
3	0.366667	0.36777	−0.30
4	0.406298	0.39956	1.66
5	0.417314	0.40905	1.98
6	0.535777	0.55299	−3.21
7	0.646354	0.63174	2.26
8	0.664218	0.63615	4.23
9	0.77137	0.75698	1.87
10	0.773718	0.76585	1.02

Table 5
Frequencies (Hz) of the simply supported stiffened plate with two stiffeners (Fig. 11, the thickness of the plate increases to 3.0 m)

Mode	ANSYS results	Present results	Relative errors to ANSYS results (%)
1	0.232308	0.22562	2.88
2	0.335349	0.32612	2.75
3	0.569531	0.54419	4.45
4	0.787483	0.75287	4.40
5	0.812595	0.82956	−2.09
6	0.886328	0.99366	−12.11
7	1.12514	1.1556	−2.71
8	1.28193	1.1679	8.90
9	1.29271	1.3781	−6.61
10	1.59458	1.3882	12.94

4.4. Simply supported stiffened plate under in-plane compression

Buckling behaviors of a series of simply supported stiffened rectangular plate under uniaxial in-plane compression (Fig. 12) have been studied. A stiffener is placed along the centre line of the plate. Both the plate and the stiffener are made of the same material with Poisson's ratio $\mu = 0.3$. The ratio of plate thickness to length is assumed to be 0.01. The buckling coefficient

$$k = \sigma_{cr} W^2 h_p/(\pi^2 D) \tag{84}$$

is computed for different plate aspect ratio L/W. σ_{cr} is the critical stress. The buckling coefficient obtained by the authors is compared with Timoshenko and Gere's derivation [4] in Figs. 13–17,

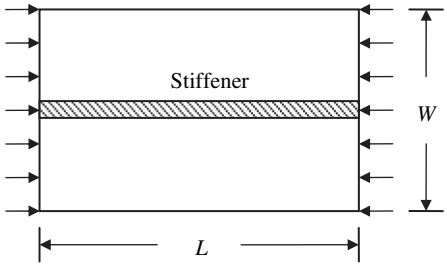

Fig. 12. A simply supported stiffened plate under in-plane compression.

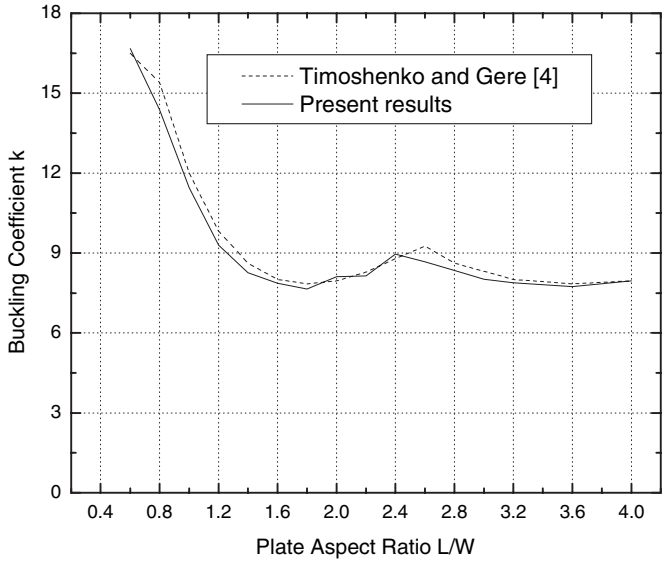

Fig. 13. Buckling coefficient of stiffened plates of different aspect ratio ($\gamma = 5, \delta = 0.05$).

where

$$\gamma = EI_{sx}/(WD) \quad \text{and} \quad \delta = W_s h_{sx}/(Wh_p). \tag{85}$$

It can be observed that most of the results are very close to those given by Timoshenko and Gere except when the plate aspect ratio is bigger than 2.8 or 3.2. Only a slight difference occurs.

4.5. Simply supported stiffened plate with two stiffeners under in-plane compression

This example is the same as in Section 4.4 except that the plate is stiffened by two stiffeners which divide the width of the plate into three equal parts (Fig. 18). The buckling coefficient obtained by the authors is compared with Timoshenko and Gere's derivation [4] in Figs. 19–22. The agreement of the two results is very good.

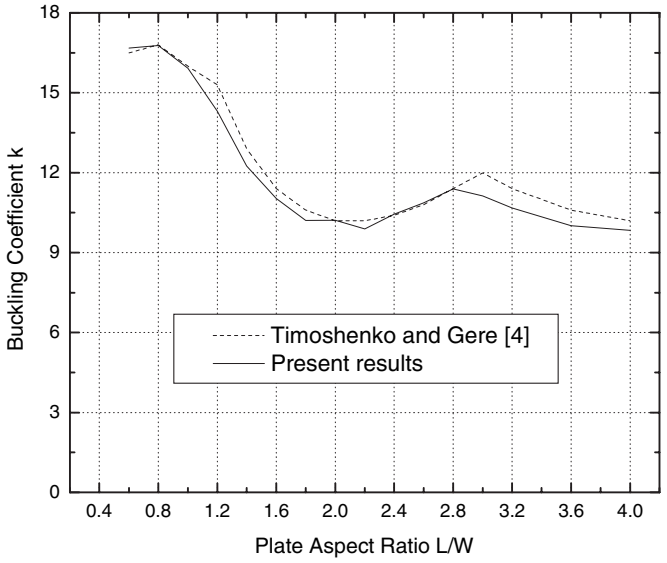

Fig. 14. Buckling coefficient of stiffened plates of different aspect ratio ($\gamma = 10, \delta = 0.05$).

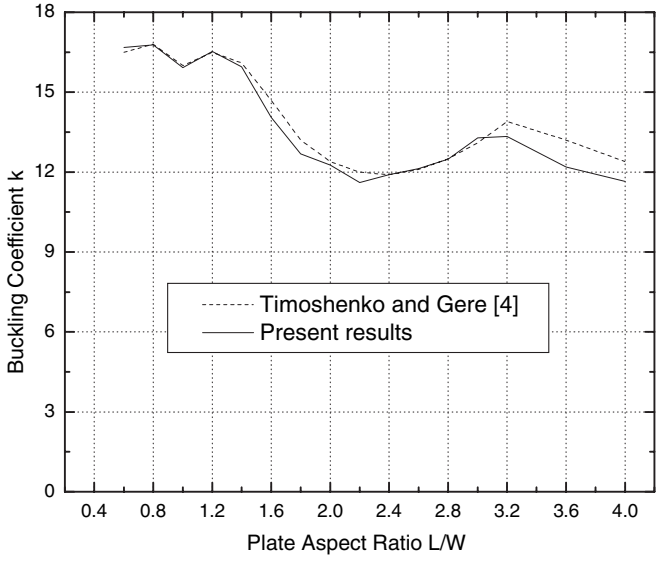

Fig. 15. Buckling coefficient of stiffened plates of different aspect ratio ($\gamma = 15, \delta = 0.05$).

4.6. *Clamped stiffened square plate with one stiffener under in-plane compression*

This example is the same as in Section 4.4 except that the plate is a clamped plate of the following non-dimensional parameters: $L/W = 1$, $\gamma = 0.2$, $\delta = 20$, $h_s = 10.483h_p$, $h_s/W_s = 2.75$, and $L/h_p = 200$. The buckling coefficients k obtained by the authors Rikards et al. [16] and Mukhopadhyay [28] are listed in Table 6.

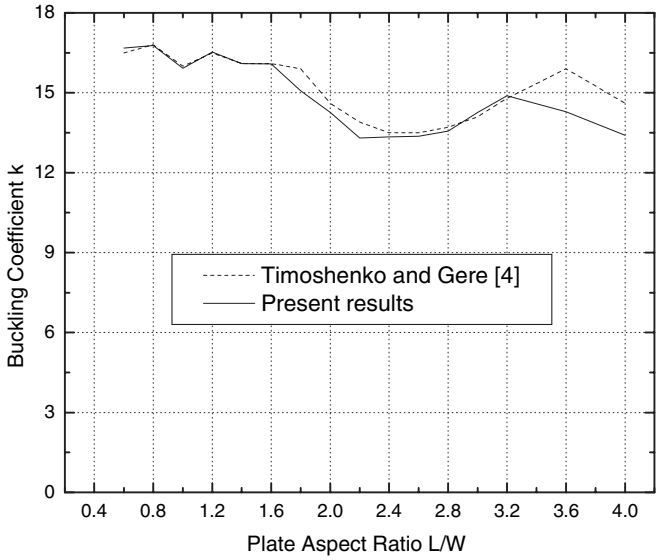

Fig. 16. Buckling coefficient of stiffened plates of different aspect ratio ($\gamma = 20, \delta = 0.05$).

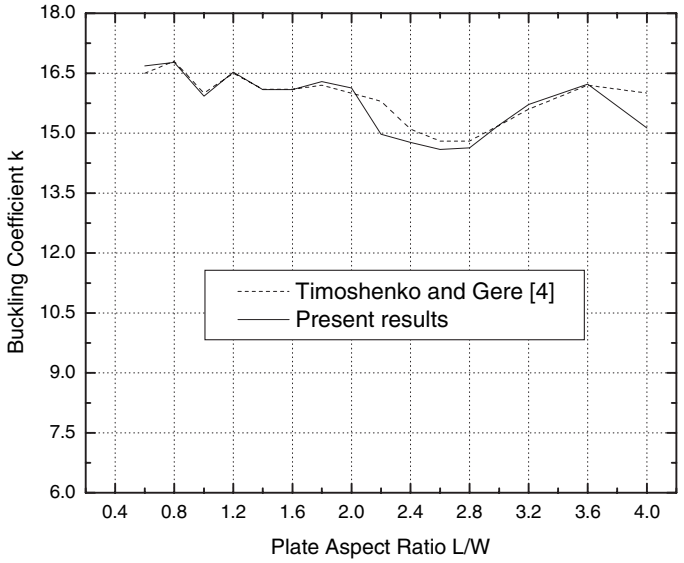

Fig. 17. Buckling coefficient of stiffened plates of different aspect ratio ($\gamma = 25, \delta = 0.05$).

4.7. Simply supported rectangular stiffened plate with two stiffeners under in-plane compressions

The stiffened rectangular plate in Section 4.3 under two direction in-plane compressions—R_x, R_y, is considered (Fig. 23). R_x is equal to R_y. The critical stress obtained by the authors is 13.71 kPa. For comparison, the authors also calculated the problem using ANSYS. The result given by ANSYS is 13.43 kPa. The same ANSYS model as in Sections 4.2 and 4.3 is used.

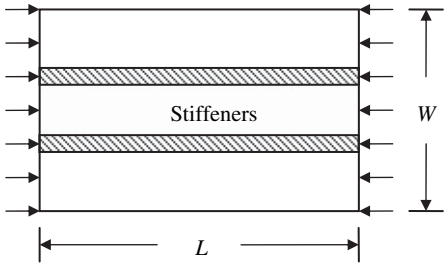

Fig. 18. A simply supported stiffened plate with two stiffeners under in-plane compression.

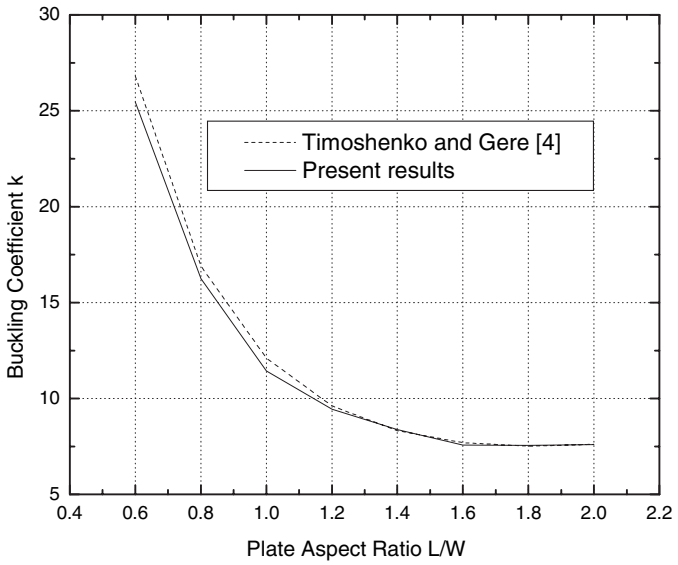

Fig. 19. Buckling coefficient of different aspect ratio plate stiffened by 2 stiffeners ($\gamma = 10/3, \delta = 0.05$).

The critical stress obtained by the authors is 193.11 kPa when the plate thickness is increased to 1.5 m. The result given by ANSYS is 196.59 kPa. When the thickness of the plate is increased to 3.0 m, the critical stress obtained by the authors is 427.8 kPa. The result given by ANSYS is 456.7 kPa.

5. Conclusions

An FSDT mesh-free method for stability and free vibration analyses of the eccentrically stiffened plate is proposed in this paper. The stiffened plate is regarded as a combination of plate and stiffeners. By employing the displacement compatible conditions in the contact surface between the plate and the stiffener, the displacement field of the stiffener is expressed in terms of the displacements of the plate. Thus, the stiffness matrix of the stiffened plate can be derived by

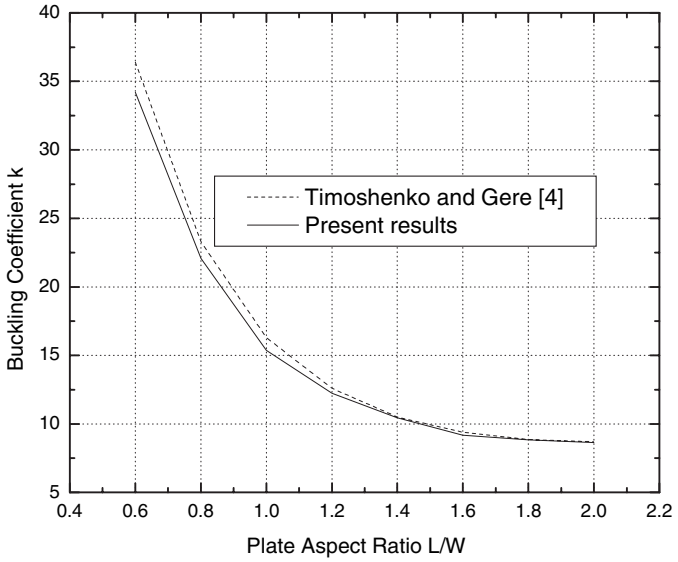

Fig. 20. Buckling coefficient of different aspect ratio plate stiffened by 2 stiffeners ($\gamma = 5, \delta = 0.05$).

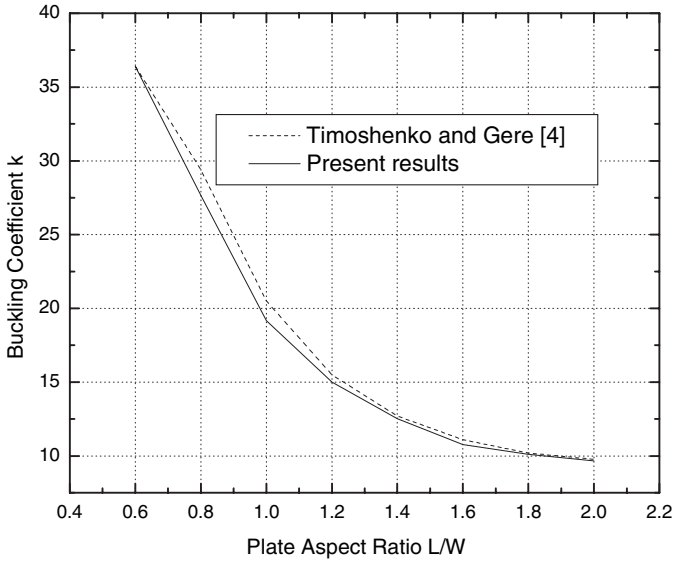

Fig. 21. Buckling coefficient of different aspect ratio plate stiffened by 2 stiffeners ($\gamma = 20/3, \delta = 0.05$).

superposing the strain energy of the plate and the stiffeners. Because there is no mesh in the meshless model of the plate, the stiffeners can be placed anywhere in the plates other than along the mesh lines and any changes of their positions will not lead to remeshing of the plate. The proposed method is checked by computing several examples. The results show good agreement with existing solutions.

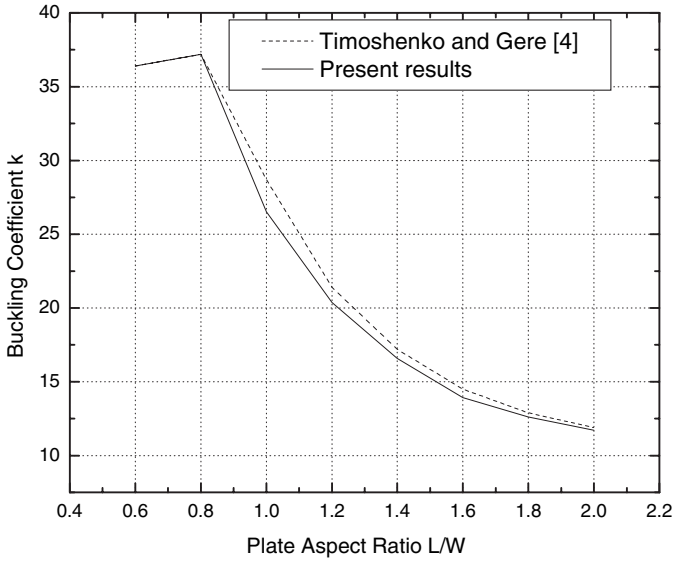

Fig. 22. Buckling coefficient of different aspect ratio stiffened by 2 stiffeners ($\gamma = 10, \delta = 0.05$).

Table 6
Buckling coefficient of the clamped stiffened plate with single stiffener

Buckling coefficient	Ref. [16]	Ref. [16] (ANSYS)	Ref. [28]	Present result
k	24.85	23.44	25.46	25.33

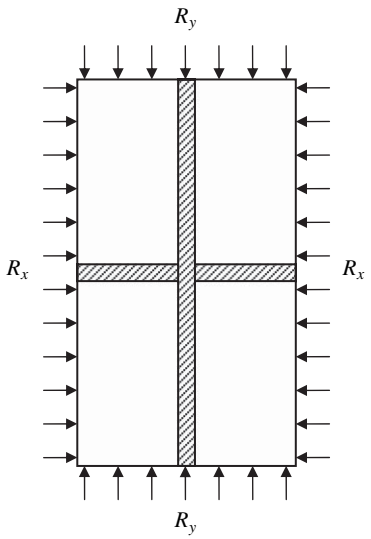

Fig. 23. The rectangular stiffened under two direction in-plane compressions.

Acknowledgements

The work described in this paper was supported by a grant from the Research Grants Council of the Hong Kong Special Administrative Region, China (Project No. CityU 1140/03E).

References

[1] H.A. Schade, The orthogonally stiffened plate under uniform lateral load, *Journal of Applied Mechanics* 62 (1940) 143–146.
[2] S. Kendrick, The analysis of a flat plated grillage, *European Shipbuilding* 5 (1956) 4–10.
[3] G.H. Bryan, On the stability of a plane plate under thrust in its own plane, with applications to the 'buckling' of the sides of a ship, *Proceedings of the London Mathematical Society* 22 (1891) 54–67.
[4] S.P. Timoshenko, J.M. Gere, *Theory of Elastic Stability*, McGraw-Hill, New York, 1961.
[5] J.M. Klitchieff, On the stability of plates reinforced by longitudinal ribs, *Journal of Applied Mechanics* 73 (1973) 364–366.
[6] G. Turvey, A Contribution to the Elastic Stability of Thin Walled Structures Fabricated from Isotropic and Orthotropic Materials, Ph.D. Dissertation, University of Birmingham, 1971.
[7] H. Yoshida, K. Maegawa, Buckling strength of orthogonally stiffened plates, *Journal of Structural Mechanics* 7 (1979) 161–191.
[8] Y.K. Cheung, C. Delcourt, Buckling and vibration of thin flat-walled structures continuous over several spans, *Proceedings of the Institution of Civil Engineers*, Part II (1977) 93–103.
[9] K.M. Liew, C.M. Wang, Elastic buckling of rectangular plates with curved internal supports, *Journal of Structural Engineering* 118 (6) (1992) 1480–1493.
[10] S. Kitipornchai, K.M. Liew, Y. Xiang, C.M. Wang, Buckling of thick skew plates, *International Journal for Numerical Methods in Engineering* 36 (1993) 1299–1310.
[11] K.M. Liew, C.M. Wang, pb-2 Rayleigh–Ritz method for general plate analysis, *Engineering Structures* 15 (1) (1993) 55–60.
[12] K.M. Liew, Y. Xiang, S. Kitipornchai, C.M. Wang, Buckling and vibration of annular Mindlin plates with internal concentric ring supports subject to in-plane radial pressure, *Journal of Sound and Vibration* 177 (5) (1994) 689–707.
[13] Y. Xiang, C.M. Wang, S. Kitipornchai, K.M. Liew, Buckling of triangular Mindlin plates under isotropic inplane compression, *Acta Mechanica* 102 (1–4) (1994) 123–135.
[14] M. Mukhopadhyay, A. Mukherjee, Finite element buckling analysis of stiffened plates, *Computers and Structures* 34 (6) (1990) 795–803.
[15] M. Guo, I.E. Harik, Stability of eccentrically stiffened plates, *Thin-Walled Structures* 14 (1992) 1–20.
[16] R. Rikards, A. Chate, O. Ozolinsh, Analysis for buckling and vibrations of composite stiffened shells and plates, *Composite Structures* 51 (2001) 361–370.
[17] M. Barik, M. Mukhopadhyay, A new stiffened plate element for the analysis of arbitrary plates, *Thin-Walled Structures* 40 (2002) 625–639.
[18] K.M. Liew, Y. Xiang, S. Kitipornchai, Research on thick plate vibration: a literature survey, *Journal of Sound and Vibration* 180 (1) (1995) 163–176.
[19] S.F. Ney, G.G. Kulkarni, On the transverse free vibration of beam-slab type highway bridges, *Journal of Sound and Vibration* 21 (1972) 249–261.
[20] T. Balendra, N.E. Shanmugam, Free vibration of plates structures by grillage method, *Journal of Sound and Vibration* 99 (1985) 333–350.
[21] C.L. Kirk, Vibration of centrally stiffened rectangular plates, *Journal of Royal Aeronautical Society* 65 (1961) 695–697.
[22] K.M. Liew, Y. Xiang, S. Kitipornchai, J.L. Meek, Formulation of Mindlin–Engesser model for stiffened plate vibration, *Computer Methods in Applied Mechanics and Engineering* 120 (3–4) (1995) 339–353.

[23] Y. Xiang, S. Kitipornchai, K.M. Liew, M.K. Lim, Vibration of stiffened skew Mindlin plates, *Acta Mechanica* 112 (1995) 11–28.
[24] Y. Xiang, K.M. Liew, S. Kitipornchai, Vibration of circular and annular plates with internal ring stiffeners, *Journal of the Acoustical Society of America* 100 (6) (1996) 3696–3705.
[25] B.R. Long, A stiffness-type analysis of the vibration of a class of stiffened plates, *Journal of Sound and Vibration* 16 (1971) 323–335.
[26] G. Aksu, R. Ali, Free vibration analysis of stiffened plates using finite difference method, *Journal of Sound and Vibration* 48 (1976) 15–25.
[27] G. Aksu, Free vibration analysis of stiffened plates by including the effect of inplane inertia, *Journal of Applied Mechanics* 49 (1982) 206–212.
[28] M. Mukhopadhyay, Vibration and stability analysis of stiffened plates by semi-analytical finite difference method—part I: consideration of bending displacements only, *Journal of Sound and Vibration* 130 (1989) 27–39.
[29] A. Mukherjee, M. Mukhopadhyay, Finite element free vibration of eccentrically stiffened plates, *Computers and Structures* 30 (6) (1988) 1303–1317.
[30] I.E. Harik, M. Guo, Finite element analysis of eccentrically stiffened plates in free vibration, *Computers and Structures* 49 (6) (1993) 1007–1015.
[31] T. Belytschko, Y.Y. Lu, L. Gu, Element-free Galerkin methods, *International Journal for Numerical Methods in Engineering* 37 (1994) 229–256.
[32] K.M. Liew, Y.Q. Huang, J.N. Reddy, A hybrid moving least squares and differential quadrature (MLSDQ) meshfree method, *International Journal of Computational Engineering Science* 3 (2002) 1–12.
[33] K.M. Liew, H.K. Lim, M.J. Tan, X.Q. He, Analysis of laminated composite beams and plates with piezoelectric patches using the element-free Galerkin method, *Computational Mechanics* 29 (6) (2002) 486–497.
[34] K.M. Liew, T.Y. Ng, Y.C. Wu, Meshfree method for large deformation analysis—a reproducing kernel particle approach, *Engineering Structures* 24 (2002) 543–551.
[35] K.M. Liew, T.Y. Ng, X. Zhao, J.N. Reddy, Harmonic reproducing kernel particle method for free vibration analysis of rotating cylindrical shells, *Computer Methods in Applied Mechanics and Engineering* 191 (2002) 4141–4157.
[36] K.M. Liew, H.Y. Wu, T.Y. Ng, Meshless method for modeling of human proximal femur: treatment of nonconvex boundaries and stress analysis, *Computational Mechanics* 28 (2002) 390–400.
[37] K.M. Liew, Y.C. Wu, G.P. Zou, T.Y. Ng, Elasto-plasticity revisited: numerical analysis via reproducing kernel particle method and parametric quadratic programming, *International Journal for Numerical Methods in Engineering* 55 (2002) 669–683.
[38] K.M. Liew, X. Zhao, T.Y. Ng, The element-free kp-Ritz method for vibration of laminated rotating cylindrical panels, *International Journal of Structural Stability and Dynamics* 2 (4) (2002) 523–558.
[39] J. Ren, K.M. Liew, Mesh-free method revisited: two new approaches for the treatment of essential boundary conditions, *International Journal of Computational Engineering Science* 3 (2) (2002) 219–233.
[40] J. Ren, K.M. Liew, S.A. Meguid, Modelling and simulation of the superelastic behaviour of shape memory alloys using the element-free Galerkin method, *International Journal of Mechanical Sciences* 44 (2002) 2393–2413.
[41] J. Wang, K.M. Liew, M.J. Tan, S. Rajendran, Analysis of rectangular laminated composite plates via FSDT meshless method, *International Journal of Mechanical Sciences* 44 (2002) 1275–1293.
[42] K.M. Liew, Y.Q. Huang, Bending and buckling of thick symmetric rectangular laminates using the moving least-squares differential quadrature method, *International Journal of Mechanical Sciences* 45 (2003) 95–114.
[43] K.M. Liew, Y.Q. Huang, J.N. Reddy, Moving least square differential quadrature method and its application to the analysis of shear deformable plates, *International Journal for Numerical Methods in Engineering* 56 (2003) 2331–2351.
[44] K.M. Liew, Y.Q. Huang, J.N. Reddy, Vibration analysis of symmetrically laminated plates based on FSDT using the moving least squares differential quadrature method, *Computer Methods in Applied Mechanics and Engineering* 192 (2003) 2203–2222.
[45] K.M. Liew, G.P. Zou, S. Rajendran, A spline strip kernel particle method and its application to two-dimensional elasticity problems, *International Journal for Numerical Methods in Engineering* 57 (2003) 599–616.

[46] X.L. Chen, K.M. Liew, Buckling of rectangular functionally graded material plates subjected to nonlinearly distributed in-plane edge loads, *Smart Materials and Structures* 13 (2004) 1–8.
[47] K.M. Liew, J. Ren, S. Kitipornchai, Analysis of the pseudoelastic behavior of a SMA beam by the element-free Galerkin method, *Engineering Analysis with Boundary Elements* 28 (2004) 497–507.
[48] K.M. Liew, X.L. Chen, Mesh-free radial basis function method for buckling analysis of non-uniformly loaded arbitrarily shaped shear deformable plates, *Computer Methods in Applied Mechanics and Engineering* 193 (2004) 205–224.
[49] K.M. Liew, X.L. Chen, Buckling of rectangular Mindlin subjected to partial in-plane edge loads using the radial point interpolation method, *International Journal of Solids and Structures* 41 (2004) 1677–1695.
[50] K.M. Liew, X.L. Chen, Mesh-free radial point interpolation method for the buckling analysis of Mindlin plates subjected to in-plane point loads, *International Journal for Numerical Methods in Engineering* 60 (2004) 1861–1877.
[51] K.M. Liew, Y.Q. Huang, J.N. Reddy, Analysis of general shaped thin plates by the moving least square differential quadrature method, *Finite Elements in Analysis and Design* 40 (2004) 1453–1474.
[52] K.M. Liew, J. Wang, T.Y. Ng, M.J. Tan, Free vibration and buckling analyses of shear deformable plates based on FSDT meshfree method, *Journal of Sound and Vibration* 276 (2004) 997–1017.
[53] K.M. Liew, J. Wang, M.J. Tan, S. Rajendran, Nonlinear analysis of laminated composite plates using the mesh-free kP-Ritz method based on FSDT, *Computer Methods in Applied Mechanics and Engineering* 193 (2004) 4763–4779.
[54] M.D. Olson, C.R. Hazell, Vibration studies on some integral rib-stiffened plates, *Journal of Sound and Vibration* 50 (1) (1977) 43–61.
[55] A. Bhimaraddi, A.J. Carr, P.J. Moss, Finite element analysis of laminated shells of revolution with laminated stiffeners, *Computers and Structures* 33 (1) (1989) 295–305.